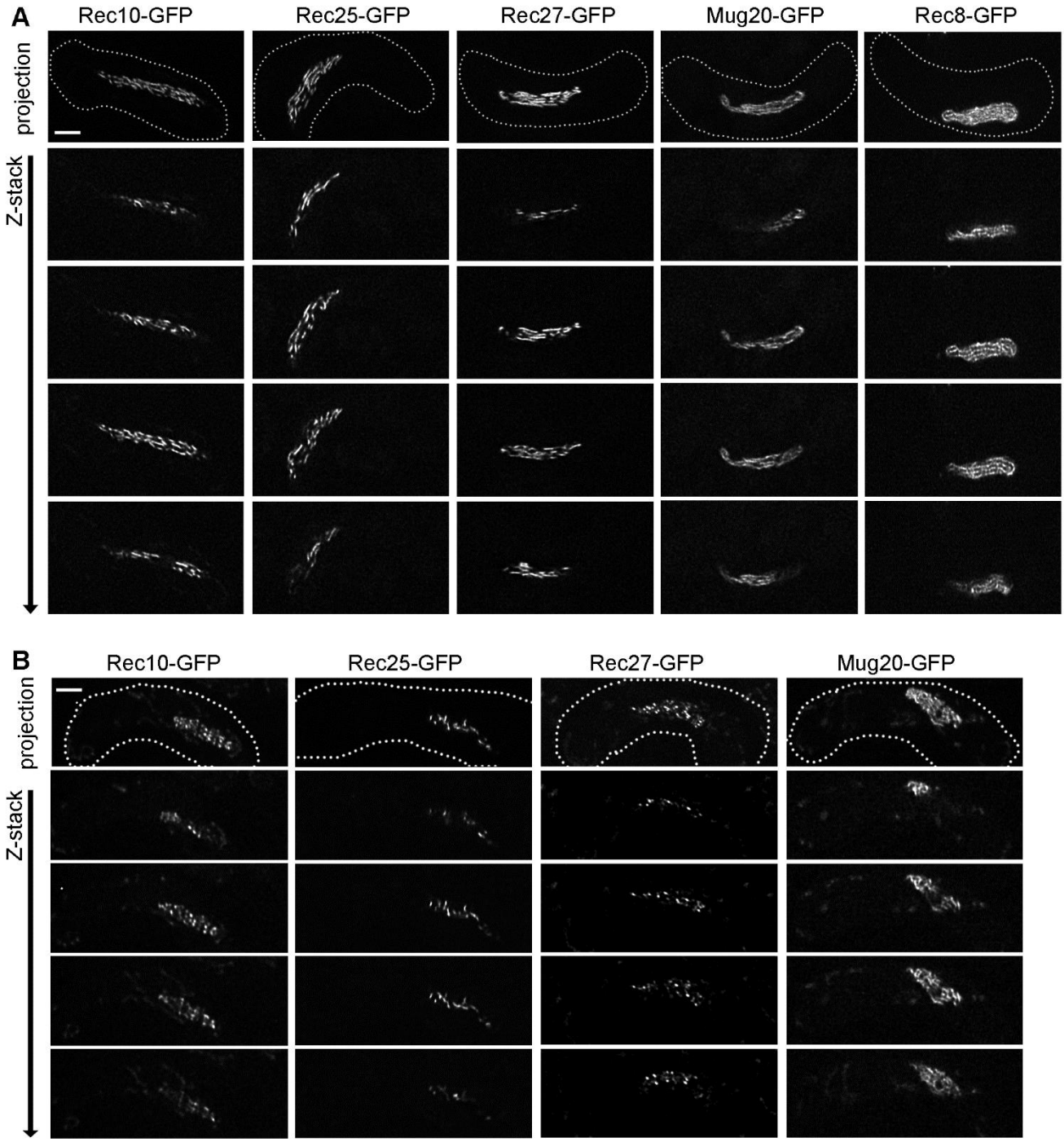

Fig. S1. LinE proteins form linear structures in zygotic meiosis at 25°C but not 34°C.
Rec10, Rec25, Rec27, Mug20 and Rec8 were observed in h^{90} strains using SIM at (**A**) 25°C or (**B**) 34°C. Each image is representative of at least 20 cells in the horsetail stage (*i.e.*, meiotic prophase; Ding et al., 2004). (A) At 25°C, all four LinEs formed elongated, linear structures; Rec8 formed bead-like linear structures. (B) At 34°C, the morphologies of Rec10, Rec-25 and Rec27 were non-continuous and often showed bright nuclear dots. These "dotty foci" were different from the "linear structures" observed at 25°C (Fig. 1A and S1A) but were similar to the structures in previous studies of azygotic meiosis at 34°C (Lorenz et al., 2004, Davis et al., 2008, Estreicher et al., 2012, Fowler et al., 2013). Mug20 showed long linear structures at 34°C, similar to those at 25°C (Fig. 1A and S1A). The top image for each strain shows the maximal projection of the entire Z-stack of image sections; representative sections are shown below. The dotted line represents the outline of the cell. The scale bar shows 2 μm. See also Fig. 1A-B.

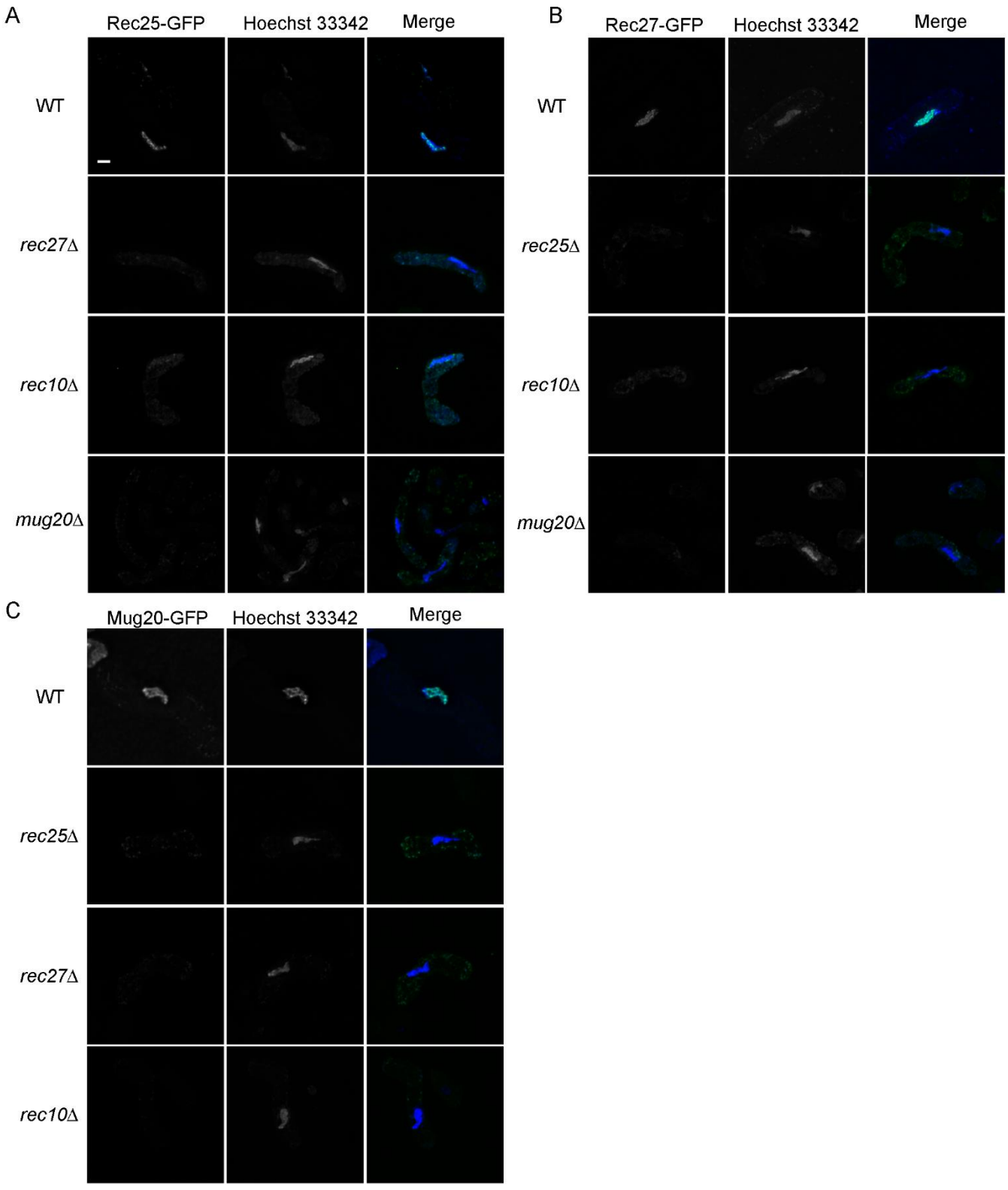

Fig. S2. Rec25, Rec27, and Mug20 nuclear structures are interdependent with other LinE subunits.

(A) Rec25, **(B)** Rec27 and **(C)** Mug20 were observed in the indicated LinE subunit mutants in h^{90} cells using DeltaVision. Each image is representative of at least 20 cells in the horsetail stage [*i.e.*, meiotic prophase (Ding et al., 2004)]. Nuclear localization is shown by Hoechst 33342 (blue) staining. The scale bar shows 2 μm.

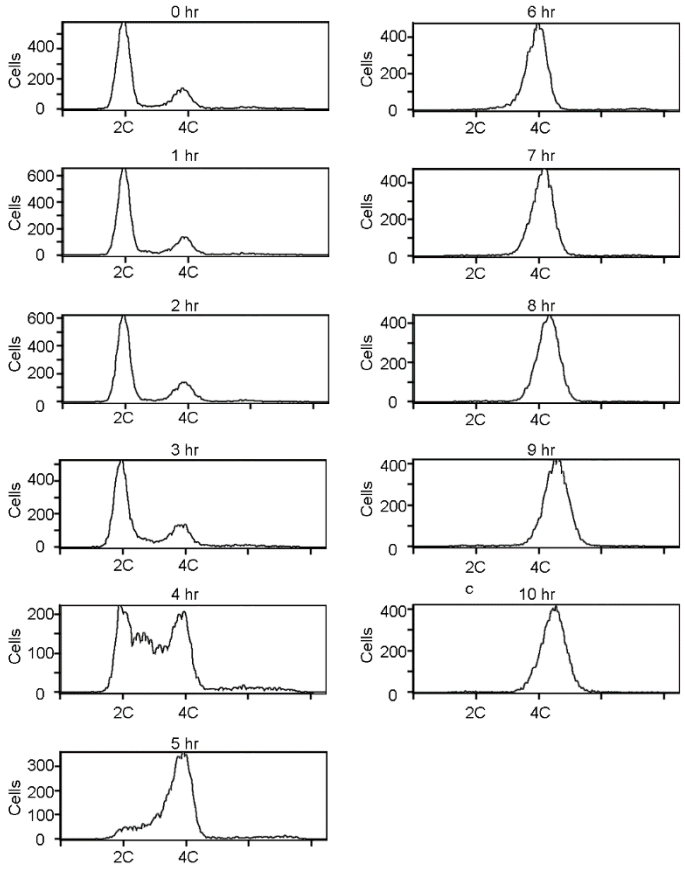

Fig. S3. Meiotic DNA replication in azygotic meiosis (*pat1-as1*) at 25°C.

DNA content of azygotic meiotic cells was analyzed by flow cytometry as described by Cervantes et al. (2000). Cells from 1 ml of meiotic culture were collected at each time point and fixed with 70% ethanol. Samples were treated with RNase for 1-2 hr, suspended in 50 mM sodium citrate (pH = 7.5) with propidium iodide (4 μg/ml) and sonicated for 30 sec before analysis in FACSCanto™ II (Becton Dickinson). The 0 hr sample was used for identifying DNA content (2C or 4C). Cells were in mid-replication at 4 hr and most cells had finished replication at 5 hr.

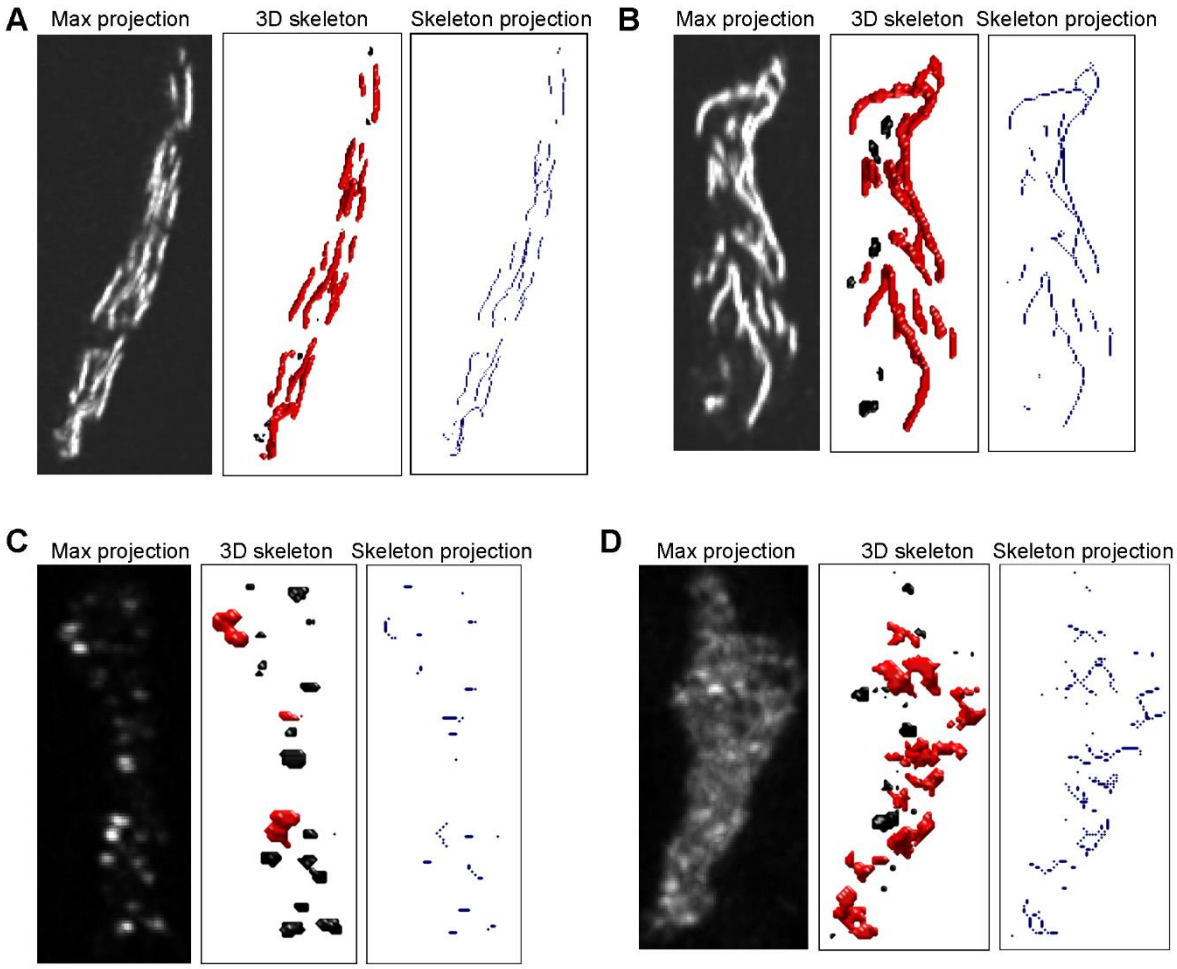

Fig. S4. Defining linear structures and dotty structures of LinE proteins.

Representative images of Rec25-GFP in (**A-B**) wild type, (**C**) *rec27-238* and (**D**) *rec27-240* in quantification analysis. Maximum projection shows the projected Z stack observed in a fluorescence microscope (SIM); 3D skeleton and skeleton projection show the 3D volume modeling and its skeletonized result (see also Materials and methods). In 3D skeleton images, elements ≥6 voxels in maximal length were painted in red. Rec25 showed more and longer linear structures in two wild-type cells (**A-B**) than in the two mutants (**C-D**), which showed mostly dotty structures. The lengths of each nuclear element in each cell are in Table S1.

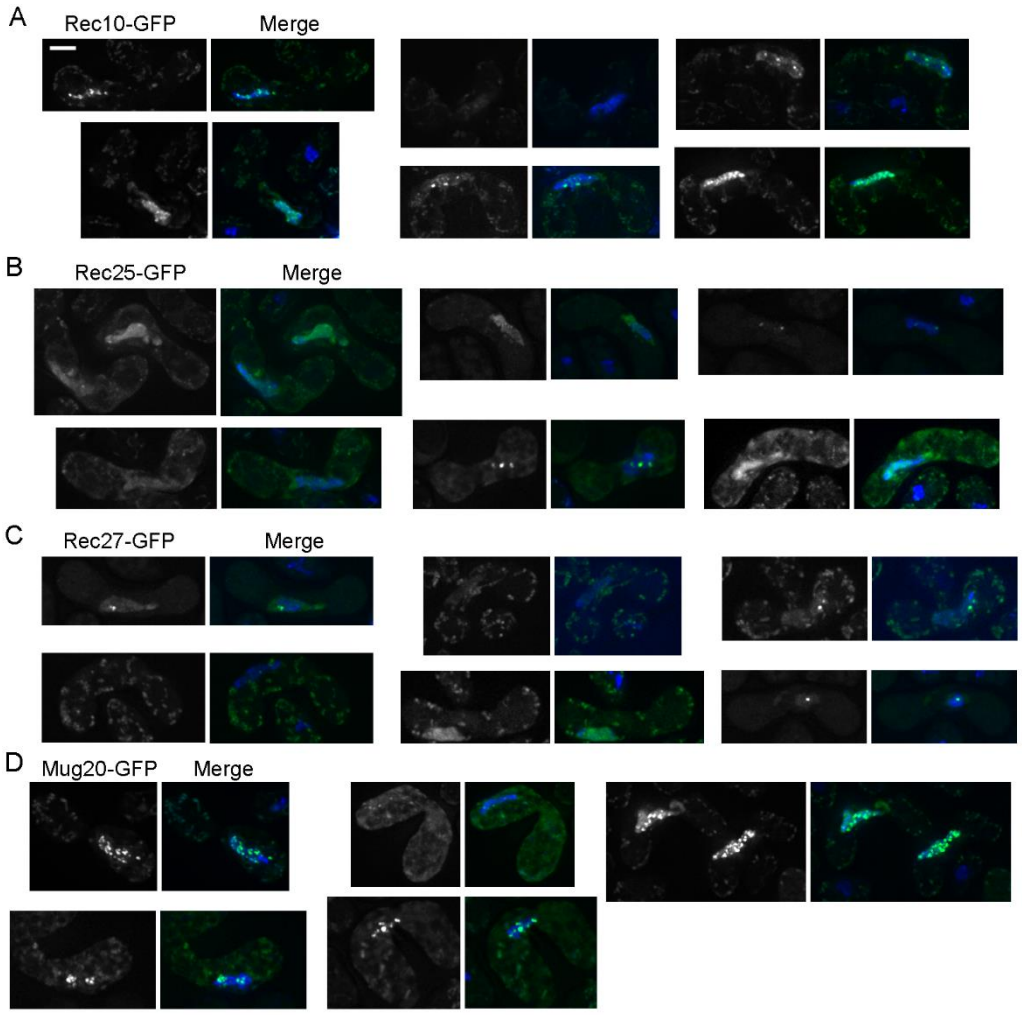

Fig. S5. LinE structures are sensitive to 1,6-hexanediol treatment.

More examples of (**A**) Rec10, (**B**) Rec25, (**C**) Rec27 and (**D**) Mug20 in h^{90} strains after 1,6-hexanediol treatment. Cells were observed by DeltaVision. 1,6-Hexanediol (10% in EMM2-N) was added for 5 min at room temperature before observation. Nuclear localization is shown by Hoechst 33342 staining. In each pair of images, the left image shows LinE-GFP, and the right image shows merged images of LinE-GFP (green) and Hoechst 33342 (blue) staining. The scale bar shows 2 μm. See also Fig. 6A-B.

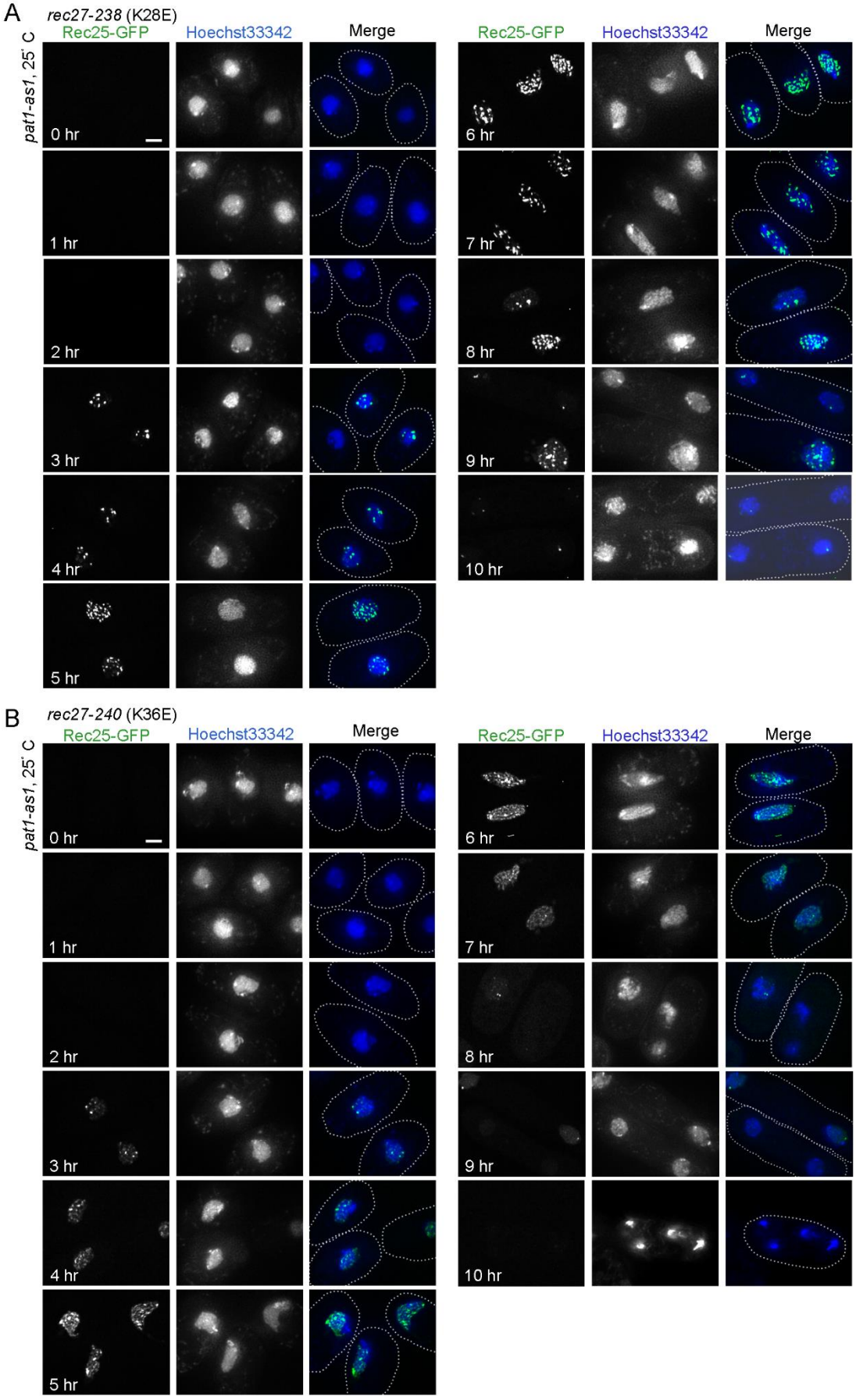

Fig. S6. Recombination-deficient LinE missense mutations alter LinE linear structures in azygotic meiosis at 25°C.

A representative LinE protein (Rec25) in (**A**) *rec27-238* (K28E) or (**B**) *rec27-240* (K38E) was observed in live cells of synchronized, azygotic meiotic cultures (*pat1-as1*) at 25°C. Cells were collected at the indicated times after meiotic induction and were observed with SIM. Each image is representative of at least 20 cells analyzed in each condition. Rec25 did not form linear configurations in either missense mutant during meiotic induction. Nuclear location is shown by Hoechst 33342 (blue) staining. The dotted line represents the outline of the cell. The scale bar shows 2 µm. See also Fig. 4 and Table S3.

Table S1. Quantification of Rec25-GFP structures in wild type and representative mutants during zygotic meiosis at 25°C[a]

	Rec25-GFP element length (voxels)			
Element number	(**A**) Wild type	(**B**) Wild type	(**C**) *rec27-238*	(**D**) *rec27-240*
1	82	117	7	22
2	51	84	7	21
3	45	65	6	19
4	35	13	5	17
5	32	11	3	14
6	32	11	3	14
7	29	8	2	12
8	27	6	2	9
9	26	5	2	8
10	19	4	2	7
11	15	2	2	6
12	12	1	2	6
13	10	1	2	2
14	10	1	2	1
15	9	1	1	1
16	6		1	1
17	4		1	1
18	3		1	1
19	2			1
20	2			1
21	2			1
22	1			1
23	1			
24	1			

[a] Quantification of Rec25-GFP nuclear elements in representative examples: (**A**-**B**) two wild- type cells, (**C**) one *rec27-238* cell and (**D**) one *rec27-240* cell. The images of fluorescence microscopy (maximum projection) and images after quantification analysis (3D skeleton and skeleton projection) are shown in Fig. S4.

Table S2. Quantification of Rec27-GFP structures during assembly and disassembly

	pat1-114, 34°C					*pat1-as1*, 25°C			
	Time course	WT	*rec12*Δ	*rad50S*	*mus81*Δ	Time course	WT	*rec12*Δ	*rec12-164*(Y98F)
Cells with foci (%)	0 hr	0±0	0±0	0±0	0±0	0 hr	0.0±0	0±0	0±0
	1 hr	0±0	0±0	0±0	0±0	1 hr	0.1±0	1.5±2	0±0
	1.5 hr	16.1±4	0±0	0±0	1.4±0	2 hr	2.3±2	0.0±0	0±0
	2 hr	70.2±5	40.9±5	61.2±2	15.8±3	2.5 hr	--	20.4±2	0±0
	2.5 hr	82.1±3	72.3±2	74.1±7	64.6±6	3 hr	72.1±9	47.2±2	68.4±2
	3 hr	85.4±2	95.6±3	81.6±4	87.1±3	3.5 hr	--	85.3±3	74.8±2
	3.5 hr	85.0±5	89.2±5	77.3±10	84.0±2	4 hr	80.1±9	92.1±3	83.6±1
	4 hr	26.6±5	76.5±7	85.9±4	95.5±2	4.5 hr	--	93.8±1	80.2±7
	4.5 hr	4.1±7	35.2±3	50.0±6	57.8±5	5 hr	87.6±2	97.6±2	84.2±5
	5 hr	1.1±6	11.3±10	27.9±4	15.0±4	5.5 hr	--	94.3±5	89.2±2
	5.5 hr	0±1	23.8±3	16.2±5	25.9±3	6 hr	92.3±2	93.4±2	90.8±2
	6 hr	0±0	0±1	0±1	0±0	6.5 hr	--	90.9±2	92.4±2
						7 hr	93.6±2	92.8±4	95.2±1
						7.5 hr	--	73.9±5	94.2±2
						8 hr	45.5±6	50.5±12	86.2±4
						8.5 hr	--	47.0±9	52.6±6
						9 hr	8.9±3	29.0±3	29.3±2
Cells with two nuclei (%)	0 hr	0±0	0.5±1	1.0±0		0 hr	1.8±1	2.6±1	0±0
	1 hr	0±0	0±0	0±0		1 hr	1.2±0	1.7±1	0±0
	1.5 hr	0.1±0	0±0	0±0		2 hr	0.0±0	0.3±0	0±0
	2 hr	0±0	0±0	0±0		2.5 hr	--	0±0	0±0
	2.5 hr	0±0	0±0	0±0		3 hr	0±0	0±0	0±0
	3 hr	0±0	0±0	0±0		3.5 hr	--	0±0	0±0
	3.5 hr	0±0	0.3±0	0±0		4 hr	0±0	0±0	0±0
	4 hr	2.2±1	5.2±2	2.0±1		4.5 hr	--	0±0	0±0
	4.5 hr	36.5±4	31.4±4	36.5±4		5 hr	0±0	0±0	0±0
	5 hr	77.6±2	70.6±3	77.6±2		5.5 hr	--	0±0	0±0
	5.5 hr	88.5±1	87.1±2	83.7±3		6 hr	0±0	0±0	0±0
	6 hr	96.1±2	95.0±0	93.0±2		6.5 hr	--	0±0	0±0
						7 hr	0±0	0±0	0±0
						7.5 hr	--	0±0	0.3±0
						8 hr	17.1±1	3.1±1	5.8±2
						8.5 hr	--	20.2±1	30.4±10
						9 hr	61.2±2	43.2±2	49.9±4
Cells with two nuclei and nuclear foci (%)	0 hr	0±0	0±0	0±0		0 hr	0±0	0±0	0±0
	1 hr	0±0	0±0	0±0		1 hr	0±0	0±0	0±0
	1.5 hr	0±0	0±0	0±0		2 hr	0±0	0±0	0±0
	2 hr	0±0	0±0	0±0		2.5 hr	--	0±0	0±0
	2.5 hr	0±0	0±0	0±0		3 hr	0±0	0±0	0±0
	3 hr	0±0	0±0	0±0		3.5 hr	--	0±0	0±0
	3.5 hr	0±0	100	0±0		4 hr	0±0	0±0	0±0
	4 hr	15.8±9	76.7±5	16.7±6		4.5 hr	--	0±0	0±0
	4.5 hr	2.3±3	35.3±6	8.5±3		5 hr	0±0	0±0	0±0
	5 hr	0±0	7.1±3	2.4±1		5.5 hr	--	0±0	0±0
	5.5 hr	0±0	0.3±1	0±0		6 hr	0±0	0±0	0±0
	6 hr	0±0	0±0	0±0		6.5 hr	--	0±0	0±0
						7 hr	0±0	0±0	0±0
						7.5 hr	--	0±0	11.1±11
						8 hr	0±0	38.7±6	42.16
						8.5 hr	--	27.3±2	24.9±2
						9 hr	0±0	18.0±3	13.1±2

Data for each parameter are the mean ± standard error of the mean ± SEM. At least 250 cells with clear nuclear staining from at least ten individual fields were examined in three experiments on different days. These data are shown in Fig. 3.

Table S3. Quantification of the length of Rec25 and Rec27 structures during a time course

	Time course	Wild type Rec27-GFP[a]	*rec27-238* Rec25-GFP[a]	*rec27-240* Rec25-GFP[a]
Maximum length[b] (voxels)	4 hr	15 ± 4 (10)[c]	18 ± 6 (4)	13 (1)
	5 hr	45 ± 7 (19)	24 ± 3 (15)	49 ± 14 (10)
	6 hr	78 ± 6 (19)	26 ± 3 (31)	47 ± 8 (14)
	7 hr	51 ± 5 (29)	24 ± 2 (30)	24 ± 7 (11)
	8 hr	35 ± 6 (8)	19 ± 3 (11)	25 ± 11 (8)
Mean of long elements[b] (voxels)	4 hr	9 ± 2	15 ± 7	9 (1)
	5 hr	21 ± 2	14 ± 2	22 ± 4
	6 hr	45 ± 9	14 ± 1	21 ± 4
	7 hr	24 ± 3	15 ± 1	13 ± 3
	8 hr	15 ± 3	14 ± 1	12 ± 4
Long elements (%)	4 hr	13 ± 3	11 ± 4	19 (1)
	5 hr	30 ± 3	20 ± 3	22 ± 5
	6 hr	36 ± 6	27 ± 2	25 ± 3
	7 hr	36 ± 4	30 ± 2	17 ± 4
	8 hr	27 ± 7	40 ± 4	13 ± 4

[a] Previous studies showed that Rec25 and Rec27 form similar nuclear structures and are required for meiotic recombination and DSB hotspot cluster formation (Davis et al., 2008, Fowler et al., 2013, Ma et al., 2017, Fowler et al., 2018). The “maximum length” and the “mean of long elements” showed no significant difference between Rec25 and Rec27 in zygotic meiosis ($p = 0.72$ and 0.40, respectively). See also Fig. 7B and Table S4.

[b] Data for each parameter are the mean ± standard error of the mean (SEM). These data are shown in Fig. 4.

[c] Number in parentheses indicates the number of cells quantified at each time point in each strain. The same cells were quantified for all three parameters.

Table S4. Quantification of the length of LinE-GFP in wild type and recombination-deficient mutants

Strain (number of cells)	Max. length (voxels)[a]	Mean of long elements (voxels)[a]
Rec25-GFP (40)[b]	72 ± 6	35 ± 4
Rec10-GFP (27)	54 ± 6	28 ± 4
Rec27-GFP (36)	68 ± 5	30 ± 4
Mug20-GFP (25)	55 ± 9	38 ± 7
rec27-238 Rec25-GFP (14)	29 ± 7	15 ± 3
rec27-239 Rec25-GFP (4)	19 ± 3	14 ± 3
rec27-240 Rec25-GFP (8)	22 ± 4	14 ± 2
mug20-251 Rec25-GFP (9)	32 ± 8	12 ± 2

[a] Data for each parameter show the mean ± standard error of the mean (SEM). These data are shown in Fig. 7B.

[b] Number in parentheses indicates the number of cells quantified for each strain. The same cells were quantified for both parameters.

Table S5. *S. pombe* strains

Strain	Genotype[a]	Used in
GP50	*h*^{90} wild type	Fig 1D, Fig 6C
GP3542	*h*^{90} *rec8::GFP-kanMX6*	Fig 1C, Fig S1, Fig 6C
GP6966	*h*$^{-}$/*h*$^{-}$ *ade6-3049/ade6-3049 pat1-114/pat1-114 rec27-205-GFP::kanMX6/rec27-205-GFP::kanMX6 lys4-95/+ +/his4-239*	Fig 2A, Fig 3A-C, Table S2
GP8762	*h*^{90} *rec10-203-GFP::kanMX6*	Fig 1A-B, Fig S1, Fig S2, Table S4
GP8766	*h*^{90} *rec25-204-GFP::kanMX6*	Fig 1A-B, Fig 5, Fig 7, Fig S1, Fig S2, Fig S4, Table S1, Table S4
GP8819	*h*^{90} *rec27-205-GFP::kanMX6*	Fig 1A-B, Fig 7, Fig S1, Fig S2, Table S4
GP8829	*h*^{90} *mug20-GFP::kanMX6*	Fig 1A-B, Fig S1, Fig S2, Table S4
GP9506	*h*^{90} *rec25-204-GFP::kanMX6 rec27-238*	Fig 7, Fig S4, Table S1, Table S4
GP9508	*h*^{90} *rec25-204-GFP::kanMX6 rec27-240*	Fig 7, Fig S4, Table S1, Table S4
GP9529	*h*^{90} *rec25-204-GFP::kanMX6 rec27-239*	Fig 7, Table S4
GP9549	*h*^{90} *rec25-204-GFP::kanMX6 rec27-184::kanMX6*	Fig S2
GP9553	*h*^{90} *rec25-204-GFP::kanMX6 mug20::natMX6*	Fig S2
GP9554	*h*^{90} *rec25-204-GFP::kanMX6 mug20-251*	Fig 7, Table S4
GP9581	*h*^{90} *rec25-204-GFP::kanMX6 mug20-250*	Fig 7
GP9591	*h*^{90} *rec27-205-GFP::kanMX6 rec25-180::kanMX6*	Fig S2
GP9592	*h*^{90} *rec10-203-GFP::kanMX6 rec25-180::kanMX6*	Fig 1E-F
GP9593	*h*^{90} *mug20-GFP::kanMX6 rec25-180::kanMX6*	Fig S2
GP9594	*h*^{90} *rec27-205-GFP:: kanMX6 mug20::natMX6*	Fig S2
GP9595	*h*^{90} *mug20-GFP::kanMX6 rec27-184::kanMX6*	Fig S2
GP9596	*h*^{90} *rec10-203-GFP::kanMX6 rec27-184::kanMX6*	Fig 1E-F
GP9597	*h*^{90} *rec27-205-GFP::kanMX6 rec10-175::kanMX6*	Fig S2
GP9598	*h*^{90} *rec25-204-GFP::kanMX6 rec10-175::kanMX6*	Fig S2
GP9599	*h*^{90} *mug20-GFP::kanMX6 rec10-175::kanMX6*	Fig S2
GP9600	*h*^{90} *rec10-203-GFP:: kanMX6 mug20::natMX6*	Fig 1E-F
GP9603	*h*$^{-}$/*h*$^{-}$ *ade6-3049/ade6-3049 pat1-114/pat1-114 rec27-205-GFP::kanMX6/rec27-205-GFP::kanMX6 rad50S/red50S lys4-95/+ +/his4-239*	Fig 3A-C, Table S4
GP9604	*h*$^{-}$/*h*$^{-}$ *ade6-3049/ade6-3049 pat1-114/pat1-114 rec27-205-GFP::kanMX6/rec27-205-GFP::kanMX6 mus81::kanMX/mus81::kanMX lys4-95/+ +/his4-239*	Fig 3A, Table S4
GP9606	*h*$^{-}$/*h*$^{-}$ *ade6-3049/ade6-3049 pat1-114/pat1-114 rec27-205-GFP::kanMX6/rec27-205-GFP::kanMX6 tel1::kanMX/tel1::kanMX rec12-169::kanMX/rec12-169::kanMX lys4-95/+ +/his4-239*	Fig 3A, Table S4
GP9647	*h*^{90} *rec27-205-GFP::kanMX6 rec25-236*	Fig 7
GP9679	*h*^{90} *rec27-205-GFP::kanMX6 rec8*$^{+}$*-mCherry-T*$_{spo5}$*<<nat*^{r}	Fig 6, Fig S5

GP9702	*h^{90} rec10-203-GFP::kanMX6 rec8^{+}-mCherry-T$_{spo5}$<<nat^{r}*	Fig 6, Fig S5
GP9703	*h^{90} rec25-204-GFP::kanMX6 rec8^{+}-mCherry-T$_{spo5}$<<nat^{r}*	Fig 6, Fig S5
GP9706	*h^{90} mug20-GFP::kanMX6 rec8^{+}-mCherry-T$_{spo5}$<<nat^{r}*	Fig 6, Fig S5
GP9748	*h^{-}/h^{-} pat1-as1(L95G)-kanMX/ pat1-as1(L95G)-kanMX rec27-302-GFP::hygMX6/ rec27-302-GFP::hygMX6 rec8-mcherry-natMX/rec8-mcherry-natMX lys4-95/+*	Fig 2B-C, Fig 3D-F, Fig 4, Fig S3, Table S4, Table S3
GP9838	*h^{-}/h^{-} pat1-as1(L95G)-kanMX/ pat1-as1(L95G)-kanMX rec25-303-GFP::hygMX6/ rec25-303-GFP::hygMX6 rec27-238/ rec27-238 lys4-95/+ +/his4-239*	Fig 4, Fig S6, Table S3
GP9858	*h^{-}/h^{-} pat1-as1(L95G)-kanMX/ pat1-as1(L95G)-kanMX rec27-302-GFP::hygMX6/ rec27-302-GFP::hygMX6 rec12-285::natMX6/rec12-285::natMX6 lys4-95/+ +/his4-239*	Fig 3D-F, Table S4
GP9866	*h^{-}/h^{-} pat1-as1(L95G)-kanMX/ pat1-as1(L95G)-kanMX rec27-302-GFP::hygMX6/ rec27-302-GFP::hygMX6 rec12-164(Y98F)/ rec12-164(Y98F) lys4-95/+*	Fig 3D-F, Table S4
GP9871	*h^{-}/h^{-} pat1-as1(L95G)-kanMX/ pat1-as1(L95G)-kanMX rec25-303-GFP::hygMX6/ rec25-303-GFP::hygMX6 rec27-240/ rec27-240 lys4-95/+ +/his4-239*	Fig 4, Fig S6, Table S3

[a] Sources of alleles other than mating type and commonly used auxotrophies are: *ade6-3049* (Steiner and Smith, 2005); *mug20-GFP::kanMX6* (Estreicher et al., 2012); *mug20::natMX6* (Estreicher et al., 2012); *mug20-250* (Ma et al., 2017); *mug20-251* (Ma et al., 2017); *mus81::kanMX* (Smith et al., 2003); *pat1-114* (Iino and Yamamoto, 1985); *pat1-as1*(L95G) (Guerra-Moreno et al., 2012); *rec8::GFP-kanMX6* (Watanabe and Nurse, 1999); *rec8^{+}-mCherry-T$_{spo5}$<<nat^{r}* (Ishiguro et al., 2010); *rec10-175::kanMX6* (Ellermeier and Smith, 2005); *rec10-203-GFP::kanMX6* (Fowler et al., 2013); *rec12-164*(Y98F) (Davis and Smith, 2003); *rec12-169::3HA-6His-kanMX6* (*rec12⊿*) (Davis and Smith, 2003); *rec25-180::kanMX6* (Martín-Castellanos et al., 2005); *rec25-204-GFP::kanMX6* (Davis et al., 2008); *rec25-303-GFP::hygMX6* (Materials and methods); *rec25-236* (Ma et al., 2017); *rec27-184::kanMX6* (Martín-Castellanos et al., 2005); *rec27-205-GFP::kanMX6* (Davis et al., 2008); *rec27-302-GFP::hygMX6* (Materials and methods); *rec27-238* (Ma et al., 2017); *rec27-239* (Ma et al., 2017); *rec27-240* (Ma et al., 2017); *rad50S* (Farah et al., 2002).

References not in main text

Davis, L., and Smith, G.R. (2003). Nonrandom homolog segregation at meiosis I in *Schizosaccharomyces pombe* mutants lacking recombination. Genetics *163*, 857-874.
Farah, J.A., Hartsuiker, E., Mizuno, K., Ohta, K., and Smith, G.R. (2002). A 160-bp palindrome is a Rad50.Rad32-dependent mitotic recombination hotspot in *Schizosaccharomyces pombe*. Genetics *161*, 461-468.
Ishiguro, T., Tanaka, K., Sakuno, T., and Watanabe, Y. (2010). Shugoshin-PP2A counteracts casein-kinase-1-dependent cleavage of Rec8 by separase. Nature Cell Biology *12*, 500- 506.
Steiner, W.W., and Smith, G.R. (2005). Optimizing the nucleotide sequence of a meiotic recombination hotspot in *Schizosaccharomyces pombe*. Genetics *169*, 1973-1983.
Watanabe, Y., and Nurse, P. (1999). Cohesin Rec8 is required for reductional chromosome segregation at meiosis. Nature *400*, 461-464.